A Sensitivity Study of Convective Cloud Formation by Vegetation Forcing with Different Atmospheric Conditions

XIAODONG HONG, MARTIN J. LEACH, AND SETHU RAMAN

Department of Marine, Earth and Atmospheric Sciences, North Carolina State University, Raleigh, North Carolina

(Manuscript received 5 April 1994, in final form 6 March 1995)

ABSTRACT

Variable vegetation cover is a possible trigger for convection, especially in semiarid areas due to differential surface forcing. A two-dimensional numerical model with explicit cloud physics and a detailed vegetation parameterization scheme is used to investigate the role of vegetation differences in triggering convective cloud formation. The ground surface in all simulations includes two irrigated vegetation areas with a dry steppe in the center of the domain. The effects of atmospheric stability, ambient moisture profile, and horizontal heating scale are investigated.

Atmospheric stability controls the growth of convective circulations. Thermal circulations form at the interfaces between the vegetated areas and the dry steppe. In the more stable environment, two distinct convective cells persist; they merge into one cell in the less stable cases. The existence of low-level moisture controls the timing and persistence of clouds that form. An interesting result is the earlier dissipation of clouds in less stable cases, as greater mixing with drier air from aloft leads to the dilution of the cloud water. Since the largest thermal forcing exists at the interfaces, length of the steppe interacts with the stability to control the merger of the cells. The two cells merge quickly into one for narrow horizontal heating. For the widest heating scale studied, no merger occurs.

1. Introduction

The incorporation of vegetation into atmospheric numerical models has received increasing attention recently because of the modification of the surface heat fluxes as compared to those from a bare soil surface with the same environmental conditions (Avissar and Pielke 1989; Noilhan and Planton 1989; Bougeault et al. 1991; Avissar and Chen 1993; Mihailović et al. 1993). Vegetated areas adjacent to dry bare soil regions provide substantial gradients of sensible heating that result in the onset of thermally induced mesoscale circulations altering the regional weather and climate (McCumber 1980; Mahfouf et al. 1987; Segal et al. 1988; Tjernstrom 1989; Pinty et al. 1989; Pielke et al. 1991; Modica et al. 1992). The intensity of the mesoscale circulation is directly related to the characteristics of the bare soil adjacent to the vegetated areas (Hong 1993) and moisture availability near the surface for evapotranspiration from the vegetation.

Rabin et al. (1990) observed that the mesoscale circulation induced by differential surface heating over regions where irrigated vegetation is adjacent to a steppe contributes to the triggering and development of convective clouds and thus increases precipitation locally. They used visible and infrared satellite images with detailed landscape information to suggest an appreciable effect of spatial variations in landscape on cumulus cloud formation over relatively flat terrain. These effects are most noticeable when forcing from the atmosphere is weak, for example, when fronts or other disturbances are absent. Clouds were observed over a mesoscale-size area (100–300 km) of harvested wheat in Oklahoma, where the ground temperature was warmer than adjoining areas dominated by growing vegetation.

Based on a theoretical study, Anthes (1984) demonstrated that the magnitudes of vertical velocities associated with this mesoscale circulation could be sufficient to trigger convective clouds. He further hypothesized that planting bands of vegetation with widths of the order of 50–100 km in semiarid regions could, under favorable large-scale atmospheric conditions, increase convective clouds and precipitation, at least locally. These increases occur through three major mechanisms: (i) increased low-level moist static energy, (ii) generation of a mesoscale circulation by differential surface heating associated with vegetation, and (iii) increased atmospheric water vapor through decreased runoff and increased evaporation. He suggested that further studies with more realistic models are necessary to obtain a definitive evaluation of the vegetation effects on the convective clouds.

A two-dimensional numerical study was performed by Yan and Anthes (1988). Their model does not have

Corresponding author address: Dr. Sethu Raman, Dept. of Marine, Earth and Atmospheric Sciences, North Carolina State University, P.O. Box 8208, Raleigh, NC 27695-8208.

vegetation explicitly although soil moisture is included. Four geometric variations of soil moisture representing vegetation coverings were used. The results supported Anthes's hypothesis and indicated that inhomogeneities in land moisture on a horizontal scale of 100–200 km can initiate convective rainfall in a convectively unstable environment with weak environmental flow and sufficient moisture.

There have been many observational and numerical studies conducted on cloud development in a conditionally unstable and moist atmosphere with triggering due to orographic lifting, surface heating, or moisture convergence (e.g., Durran and Klemp 1982; Banta 1990). However, very few studies have focused on the vegetation triggering mechanism for convective clouds either through observations or with models. This triggering is particularly important in regions where cool, irrigated vegetation abuts hot, dry bare soil. This contrast is common during summer in agricultural areas such as the western United States (Doran et al. 1992), the San Joaquin and Sacramento Valleys, and other subtropical and midlatitude geographical locations (Segal et al. 1988).

This paper investigates the role of vegetative covering as a triggering mechanism in generating convective clouds using a two-dimensional mesoscale numerical model, including a vegetation parameterization scheme and an explicit cloud physics scheme. Two effects will be investigated: (i) the effect of vegetation forcing as a triggering mechanism on convective cloud formation under different atmospheric environments and (ii) the effect of surface differential heating scales on convective cloud formation. To achieve the first goal, atmospheric stability and moisture are varied for the planetary boundary layer (PBL) and a layer above. Three regimes of atmospheric stabilities—absolutely stable, conditionally unstable, and neutral in lower atmosphere with absolutely stable or conditionally unstable condition aloft—are considered as the initial environment with a moist atmosphere in the lower layers. Variation of the atmospheric moisture in the lower layers is studied with two regimes of atmospheric stability, one of which is absolutely stable and the other conditionally unstable. Moisture in the upper levels is also considered with the three regimes of static stabilities mentioned above. To achieve the second goal, sizes of a single strip of steppe surrounded by irrigated vegetation are varied.

2. Model description

The two-dimensional mesoscale numerical model is based on the model originally developed by Huang (1990) and Huang and Raman (1991a,b). The model has been used in several numerical experiments (Huang and Raman 1991a,b, 1992; Boybeyi and Raman 1992) to demonstrate its validity with different meteorological conditions and topographic features. The model is hydrostatic and anelastic and uses a terrain-following coordinate system. The features of the model include the following.

1) *PBL parameterization.* The atmospheric PBL is treated as the surface layer and the transition layer, separately. The similarity stability functions given by Businger et al. (1971) as modified by Louis (1979) are used to account for the surface-layer turbulent transport. The turbulence closure scheme used for the transition layer is based on a prognostic equation for the turbulence kinetic energy (TKE) with the level 2.5 formulation of Mellor and Yamada (1982) for the eddy diffusivity. The height of PBL is calculated using the relationship suggested by Deardorff (1974) for convective conditions, which includes the effects of entrainment.

2) *Radiative transfer.* The radiative scheme incorporates longwave and shortwave radiative transfer. It is essentially the one used by Mahrer and Pielke (1977). This scheme accounts for absorption of shortwave radiation by water vapor and the longwave energy emitted by water vapor and carbon dioxide. The net shortwave radiation and the net longwave radiation received on the top of vegetation layer are computed following Paltrige and Platt (1976). The cloud effects on radiation have been included following Kasten and Czeplak (1980).

3) *Numerical techniques.* An upstream cubic spline is used for horizontal advection (Pielke 1984), and a quadratic upstream interpolation is used for vertical advection. The vertical diffusion terms for subgrid-scale fluxes are represented by a semi-implicit scheme (Paegle et al. 1976).

The model has been modified to include five category cloud physics and surface energy budget. The model equations after modification are given in the appendix. The detailed description of the modified version of the model can be found in Hong (1993) and Leach (1994). A brief description of the model with the modifications incorporated for this study is given below.

1) *Cloud microphysics.* The cloud microphysics parameterization is a five category (water vapor, cloud water, rainwater, cloud ice, and snow) bulk water scheme based on the work of Rutledge and Hobbs (1984). In a bulk water scheme, cloud microphysical processes that transfer water substance from one phase to another are parameterized, and particle size distributions are assumed to be continuous. The thermodynamic forcing due to phase changes of water is parameterized to consider the condensation or evaporation of cloud water, evaporation of rainwater and melting snow, initiation of cloud ice, depositional growth of cloud ice and snow, melting of snow and cloud ice, and collection of cloud water by snow. The transfer (sources and sinks) between any two phase categories is parameterized to include the autoconversion of cloud water, collection of cloud water by rain-

water, collection of cloud ice by snow, and conversion of cloud ice by snow. The removal of water by precipitation processes is zero for water vapor, cloud water, and cloud ice and is parameterized with a mass-weighted fall velocity for rain and snow. The detailed description of parameterization for these source or sink terms can be found in Leach (1994).

2) *Vegetation inclusion.* The vegetation parameterization of Deardorff (1978) for the surface energy budget has been included in the model. This scheme provides for heat and water exchanges at the land–atmosphere interface with a representation of a single vegetation layer and two soil layers. Evapotranspiration is determined as if the plant canopy were no more than a partly wet plane at the lower boundary of the atmosphere. Plant evaportranspiration can be expressed in terms of measurable weather parameters together with the physiological and aerodynamic resistance. Plant transpiration requires energy to supply the latent heat of conversion of water from the liquid to the vapor phase and also involves diffusion of water vapor away from the transpirating surface. A bulk stomatal resistance for diffusion from the evaporating sites within the leaf to the leaf surface and a bulk aerodynamic resistance for diffusion from the surface to the well-mixed surrounding air are included. The saturation deficit is used to calculate evaporation or condensation from or onto the leaf. Condensation that occurs on the soil surface is not treated as dew but is simply added to the bulk soil moisture budget. The ground surface temperature and soil moisture are obtained by solving simultaneously the energy budget and water budget equations at the soil–vegetation–air interface, respectively. The detailed description of vegetation parameterization can be found in Hong (1993).

3. Computational aspects

a. Boundary conditions

Orlanski's radiation condition (Orlanski 1976) with a forward-upstream formulation (Miller and Thorpe 1981) is applied at the lateral inflow boundaries, while the prediction equations with a forward-upstream differencing are used at the lateral outflow boundaries. At the lower boundary, a no-slip condition is imposed. The hydrostatic equation is used to obtain the surface pressure with the known upper-level pressure. At the upper boundary, the prediction equations with a forward-upstream differencing scheme are used for both outflow ($w > 0$) and inflow ($w < 0$) grids, except for the vertical advection terms that are represented by the interior grid nearest the boundary using upstream differencing. An upper boundary condition allowing internal gravity wave radiation (Klemp and Durran 1983) is employed.

b. Initial conditions

In order to obtain the initial fields for the numerical simulation, the Ekman gradient equation is solved with the zonal and longitudinal geostrophic wind components, respectively. A uniform surface potential temperature is specified initially, and the vertical profile is obtained by thermal wind balance.

c. Model parameters

The model domain is 360 km × 7 km in the horizontal and vertical, with a uniform horizontal grid length of 4 km. There are 18 vertical layers at 0, 30, 60, 100, 200, 400, 700, 1000, 1500, 2000, 2500, 3000, 3500, 4000, 4500, 5000, 6000, and 7000 m. Choice of the vertical spacing is not critical in numerical simulations because of the use of an implicit scheme for the vertical diffusion terms. The model domain has been designed to represent two irrigated vegetation areas in both sides of the domain separated by dry bare soil (steppe). The widths of the irrigated vegetation and steppe are 140 and 80 km, respectively, for cases 1–4, and varying widths for case 5 (as shown in Table 1). The solar radiation parameters correspond to 15 June at a latitude of 45.83°N. The design of the domain, the day of the year, and the latitude chosen are consistent with the Boardman Regional Flux Experiment

TABLE 1. The numerical experiments for the variation of atmospheric stability, moisture, and surface heating scales.

	PBL	Above PBL
Case 1 (Variation of atmospheric stability with 90% relative humidity in the PBL and 0% above PBL)		
(a)	Absolutely stable	Absolutely stable
(b)	Conditionally unstable	Conditionally unstable
(c)	Neutral	Absolutely stable
(d)	Neutral	Conditionally unstable
Case 2 (Variation of atmospheric moisture with absolutely stable atmospheric condition)		
(a)	50% relative humidity	0% relative humidity
(b)	70% relative humidity	0% relative humidity
(c)	80% relative humidity	0% relative humidity
(d)	100% relative humidity	0% relative humidity
Case 3 (Variation of atmospheric stability with 90% relative humidity in the PBL and 45% above PBL)		
(a)	Absolutely stable	Absolutely stable
(b)	Conditionally unstable	Conditionally unstable
(c)	Neutral	Absolutely stable
(d)	Neutral	Conditionally unstable

Case 4 (Variation of surface heating scales with absolutely stable atmospheric condition and high moisture content)	Irrigated vegetation	Steppe	Irrigated vegetation
(a)	170 km	20 km	170 km
(b)	160 km	40 km	160 km
(c)	140 km	80 km	140 km
(d)	120 km	120 km	120 km

TABLE 2. Vegetation and soil characteristics.*

	Value
Irrigated vegetation	0.17
Canopy albedo	
Canopy emissivity	0.98
Roughness length (m)	0.056
Minimum stomatal resistance (s m^{-1})	50
Leaf-shielding factor	0.8
Depth of root layer (m)	0.6
Initial surface soil moisture (m^3 m^{-3})	0.17
Initial root-layer soil moisture (m^3 m^{-3})	0.25
Soil thermal diffusivity ($\times 10^{-6}$ m^2 s^{-1})	0.74
Dry volumetric heat capacity ($\times 10^6$ J m^{-3} K^{-1})	2.96
Ground surface temperature (K)	291
Steppe (dry bare soil)	1.00
Soil emissivity	
Leaf shielding factor	0.0
Soil albedo	0.25
Roughness length (m)	0.02
Depth of deep layer (m)	0.6
Initial surface soil moisture (m^3 m^{-3})	0.03
Initial deep-layer soil moisture (m^3 m^{-3})	0.05
Soil thermal diffusivity ($\times 10^6$ m^2 s^{-1})	0.24
Dry volumetric heat capacity ($\times 10^6$ J m^{-3} K^{-1})	1.28
Ground surface temperature (K)	291

* Data are referenced from Pinty et al. (1989) and Pielke (1984).

(Doran et al. 1992), a field campaign designed to study the effects of subgrid-scale variability of sensible and latent heat fluxes on the boundary layer properties. The area for this experiment consists of two principal land types—hot, dry steppe and cool, moist farmland. The domain size used in this study is, however, larger.

The initial ground surface temperature and the mean deep soil temperature are based on the observations by Doran et al. (1992). The initial wind speed is 0.01 m s^{-1} for a weak large-scale atmospheric disturbance (Rabin et al. 1990). The unidirectional environmental wind is a constraint of a slab symmetric model. Two-dimensional modeling of three-dimensional dynamics of convective clouds confining the flow to a vertical plane affect the realistic simulation of updrafts and downdrafts and could overestimate the magnitude of perturbation pressure forces (Rogers and Yau 1989; Houze 1993). This is a constraint that should be considered in analyzing the results.

The soil properties and vegetation parameters used for the simulations are shown in Table 2. The data for irrigated vegetation is taken from Pinty et al. (1989) and for soil property from Pielke (1984). The time step for all simulations is 20 s. The starting time of the experiments is 0800 LT. Results for an integration time of 6 h is chosen based on the consideration of a typical surface heating cycle, similar to the land sea breeze.

d. Design of experiments

Four cases were simulated to study the vegetation forcing that triggers convective clouds under different atmospheric environments. The four cases include varying the atmospheric stability and moisture. The atmospheric stabilities and moisture variation used for each case are given in Table 1. Variations in the width of the steppe to examine the effect of different surface heating scales is also given on Table 1 for case 5.

4. Discussion of experimental results

a. The influence of atmospheric stability on clouds triggered by vegetation forcing (case 1)

Idealized cases are investigated to show how the stability of the atmosphere interacts with a mesoscale circulation induced by differential surface heating. The effects of stability on clouds triggered by the circulations are investigated by studying three atmospheric stability regimes in the lower atmosphere: an absolutely stable, a neutral, and a conditionally unstable atmosphere (Fig. 1). For further comparison purposes, two stabilities in the layer above the neutral boundary layer, an absolutely stable and a conditionally unstable layer, are considered.

An absolutely stable environment generally occurs during early mornings when large radiational cooling under clear skies leads to the creation of a stable layer at the surface. A conditionally unstable atmosphere exists when the tropospheric lapse rate, though stable, is less than moist adiabatic. This condition is often met during the warm season in arid or semiarid regions such as the western United States because of the latent heat and high sensible heat fluxes. Near-neutral at-

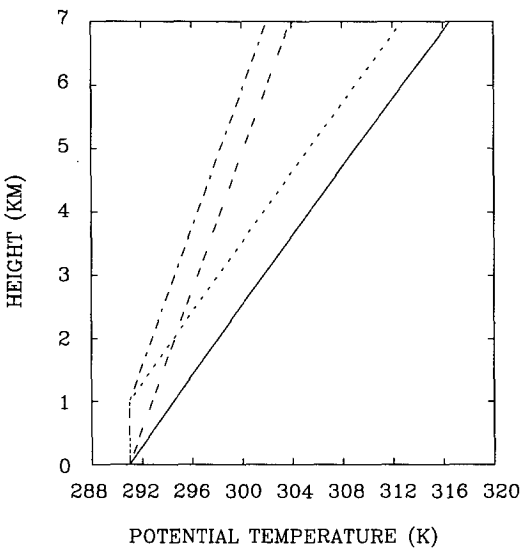

FIG. 1. The potential temperature profiles used to initialize the model for various cases. The solid line is the absolutely stable case, the long dashed line is the conditionally unstable case, the dashed line is a neutral boundary layer case with an absolutely stable layer aloft, and the alternating dashed dot line is a neutral boundary layer with a conditionally unstable layer aloft.

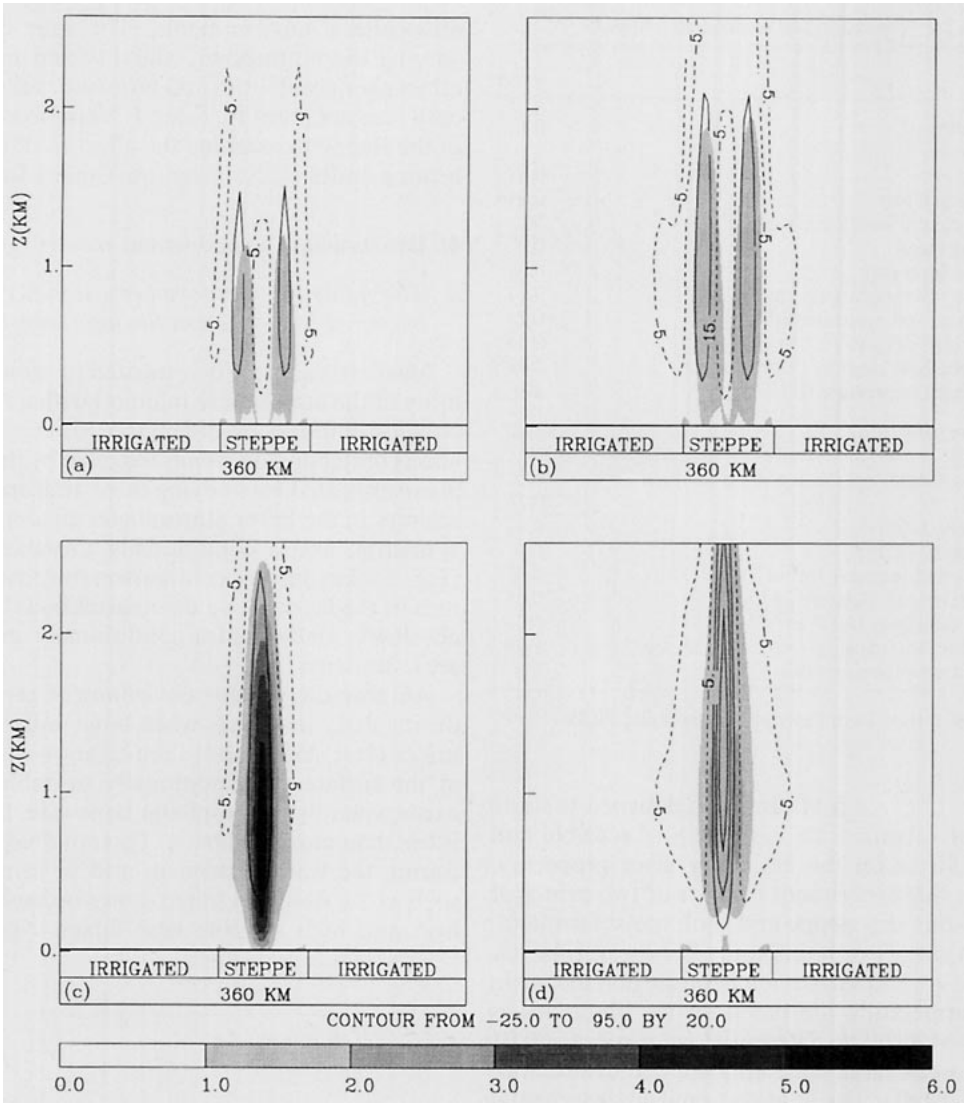

FIG. 2. The vertical velocity w (cm s^{-1}) are overlaid on TKE (m^2 s^{-2}) for case 1: (a) absolutely stable, (b) conditionally unstable, (c) neutral boundary layer with an absolutely stable layer aloft, and (d) neutral boundary layer with a conditionally unstable layer aloft. The initial moisture in all cases was 90% relative humidity in the boundary layer with dry conditions aloft. The gray-scale bar at the bottom indicates the range and shading values for the TKE.

mospheric conditions in the boundary layer exist with overcast skies and strong surface geostrophic winds. In the cases we describe here, the boundary layer is initially 1 km deep with 90% relative humidity. The air above the boundary layer is dry with a relative humidity of 0%. This creates a negative $d\theta_e/dz$ (θ_e is the equivalent potential temperature), that is, a potentially unstable atmosphere.

A thermally induced mesoscale circulation is created due to the differences in surface forcing between a vegetated area and bare soil and disrupts a stably stratified atmosphere, forcing vertical displacement of the air trajectories. The initial lapse rate becomes less stable, for all cases. However, the ability of air to ascend remains less with more stable initial conditions. Figure 2 shows the turbulence kinetic energy (TKE) in gray scale with contours of the vertical velocity overlaid. The four panels are for different initial stability profiles, representing (a) a stable atmosphere, (b) a conditionally stable atmosphere, (c) a neutral lower atmosphere (lowest 1000 m) with an absolutely stable upper atmosphere, and (d) a neutral lower atmosphere with a conditionally stable upper atmosphere. For the stable lower atmosphere (Fig. 2a) and conditionally stable lower atmosphere (Fig. 2b), two updrafts form with a subsiding region between the updrafts. The magnitudes of the vertical component are larger for the less stable case. This is expected since with greater stability and

therefore greater restoring force, smaller amplitude buoyancy-generated disturbances occur. The single convective cell generated in the neutral case is also consistent with these stable cases. A smaller restoring force allows larger amplitude disturbances to develop in the less stable cases. With even less restoring force in the lower atmosphere, the amplitude and wavelength of the generated disturbance is such that no downdraft is generated between the two convectively generated cells at the surface, and the two cells merge (Fig. 3). It is the difference in surface forcing that drives the low level convergence and the resulting updrafts. The weaker restoring force allows the two cells to merge into one updraft earlier. The convergence of the two cells toward the center in the weak stability cases is consistent with the result of Yan and Anthes (1988).

Stronger surface convergence exists with the unstable and neutral initial conditions. Deeper convection cells appear in these cases resulting from the stronger turbulent mixing in the boundary layer. The two updrafts in the stable and weakly stable cases are clearly evident in the TKE distribution. The maximum value of TKE occurs for the neutral case with an overlying absolutely stable atmosphere (shown in Fig. 2c). The TKE is transported through greater depths when a conditionally unstable atmosphere is above the neutral boundary layer (Fig. 2d). The TKE transport is most likely due to the turbulent transport term. Because of the transport through greater depths, the maximum value of TKE is larger for the case illustrated in Fig. 2c, but larger amplitude disturbance exists with smaller upper-layer ambient stability.

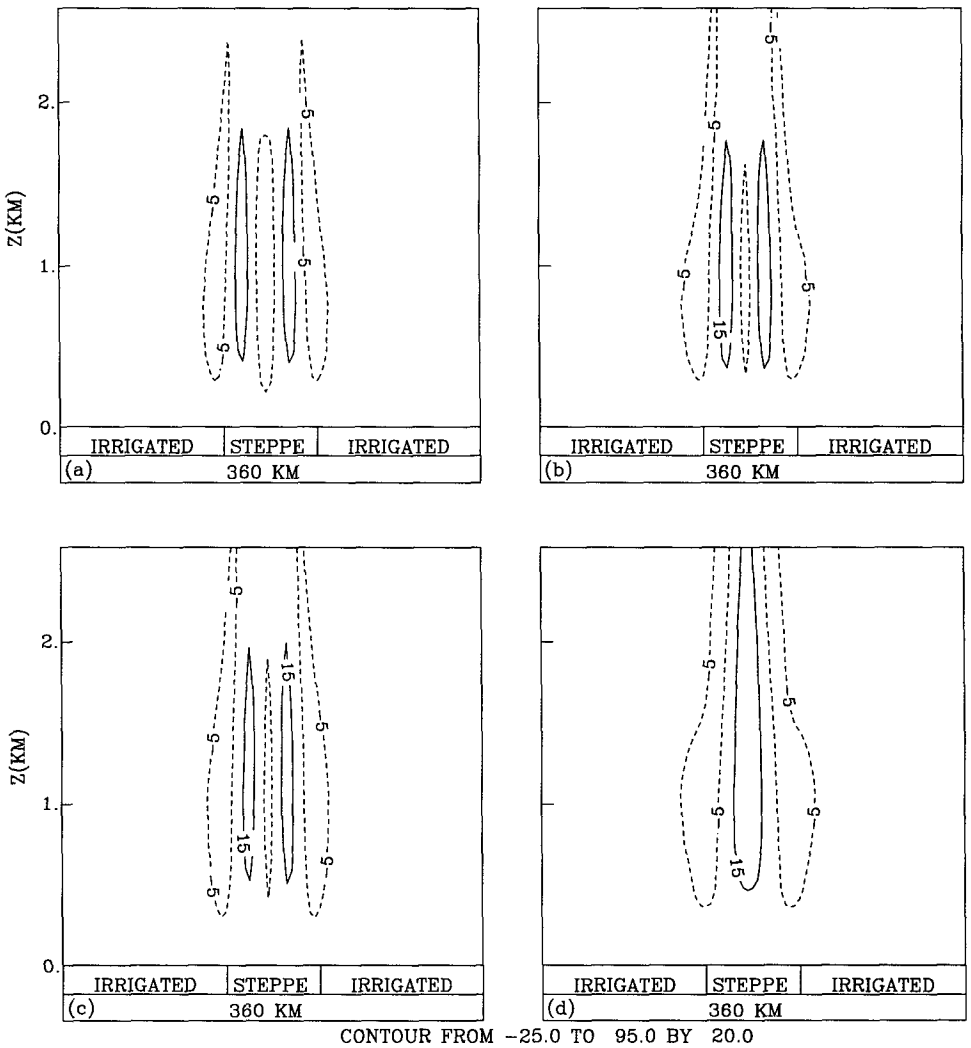

FIG. 3. The vertical velocity w (cm s^{-1}) for case 1c with the neutral boundary layer and an absolutely stable layer aloft: (a) after 4-h simulation, (b) after 5-h simulation; and for case 1d with the neutral boundary layer and a conditionally unstable layer aloft: (c) after 4-h simulation, (d) after 5-h simulation.

The cloud water in gray scale with contours of equivalent potential temperature θ_e overlaid are shown in Fig. 4 for case 1. The stability decreases progressively from Figs. 4a–d. The results shown in Fig. 4 are consistent with those discussed above. The increasing amplitude of the generated disturbance with decreasing stability is seen by examining the θ_e profiles. The bimodal characteristic of the disturbance in the more stable case is also evident from the θ_e fields.

Clouds appear here only for the initially stable condition (Fig. 4a). A conditionally unstable temperature lapse rate is developed by destabilizing the absolutely stable layer. Suppressed vertical (or turbulent) mixing of heating and moisture with a more stable initial condition creates a large negative lapse rate of θ_e and hence convective instability. The maximum negative $d\theta_e/dz$ occurs in the cloud layer, and the upper stable layer limits further moisture transfer in the vertical direction. If a layer with sufficient potential instability and moisture is lifted such that a portion of the layer (at least a few hundred meters deep) becomes saturated, then the triggering of the potential instability leads to cloud formation. Low-level convergence forces the layer ascent bringing air parcels to saturation. Strong vertical turbulent mixing over the bare soil lifts air masses, which includes background moisture, and provides the condition for producing saturation (Fig. 4a). Sufficient moisture and strong convective instability combined with the thermally induced circulation in the low layers creates adequate conditions to generate clouds when the initial environment is absolutely stable. Cloud develops in the strongest convergence region as more moist air is brought from vegetated area to supply moisture needed for cloud formation.

The cloud formation mechanism also explains why no clouds are generated for the other initial conditions that were stable. Vertical moisture transfer is related to upward motion and turbulent mixing. Initially unstable and neutral conditions generate more turbulent mixing early before the thermally induced circulation develops because of preexisting instability. The effect of vigorous turbulent mixing can be inferred from the TKE distribution in Figs. 2b–d. Moisture is redistributed through the boundary layer due to the turbulent mixing. The greater turbulent mixing in the less stable case leads to a deeper well-mixed layer and the dilution of the water vapor. The greatest concentration of water vapor is found in the more stable case, and clouds form if saturated. However, integrated water vapor amounts for the cases are similar. Less moist static energy exists in the lower layer because it is related to the vertical stratification of water vapor. A weaker convective instability in the cloud layer can be seen by the small negative lapse rate of θ_e (Figs. 4b–d). Moisture is then inadequate and cloud formation is inhibited, although sufficient lifting forces are generated.

Fogs form only over the vegetated area due to increased latent heat flux (Fig. 4). Approximately the same amount of solar radiation is received at the surface over both the dry soil and the vegetated area. More shortwave radiation is absorbed by the vegetation as the albedo of the vegetated soil is smaller than that over the steppe (Table 2). However, more energy is partitioned into latent heat flux (Segal et al. 1988; Tjernström 1989; Hong et al. 1994), thus increasing the moisture content in the lower atmosphere. At the same time, larger sensible heat flux over the steppe leads to the mesoscale circulation, which in turn induces subsidence over the vegetated area (Fig. 2). The subsidence inhibits vertical mixing and causes a lowering of the boundary layer depth, evident from the plots of equivalent potential temperature (Fig. 4). The combination of surface moisture flux, reduced mixing, and a smaller mixing depth leads to the saturation of the air near the surface as lower atmosphere was initially close to saturation.

The horizontally averaged, vertically integrated cloud water C_{ave}, maximum value of cloud water C_{max}, turbulence kinetic energy TKE_{max}, and vertical velocity W_{max} for the same experiments are presented in Fig. 5. The experiments are represented by dashed and dotted lines as described in the figure caption. The horizontally averaged, vertically integrated cloud water is defined as

$$C_{\text{ave}} = \frac{\int \left[\int \rho q_c dz \right] dx}{\int dx}, \qquad (1)$$

where ρ is air density (kg m^{-3}) and q_c is cloud water (g kg^{-1}). The limits of integration are the entire domain depth and length.

The horizontally averaged, vertically integrated cloud water increases with time for all conditions, as shown in Fig. 5a. There is more cloud water at early times for the near neutral conditions, and the increase in cloud water amount is greater for the stable case. There is very little generation of new cloud for the neutral cases. The increase of cloud water in the conditionally unstable case is closer to the stable case, although the growth at later times is much less. This is due to the dilution effects, as the water vapor is mixed through greater depths as compared to the stable case. Figure 5b shows the maximum value of cloud water that exists in any cell in the model domain for case 1. The gradual decrease for both neutral cases, together with the gradual increase in total cloud water seen in Fig. 5a, indicates again that mixing dilutes the clouds through greater depths. The rapid increase in maximum cloud water for the stable case further illustrates the dilution effects. In stable conditions, there is less mixing, and therefore the cloud that does exist is more

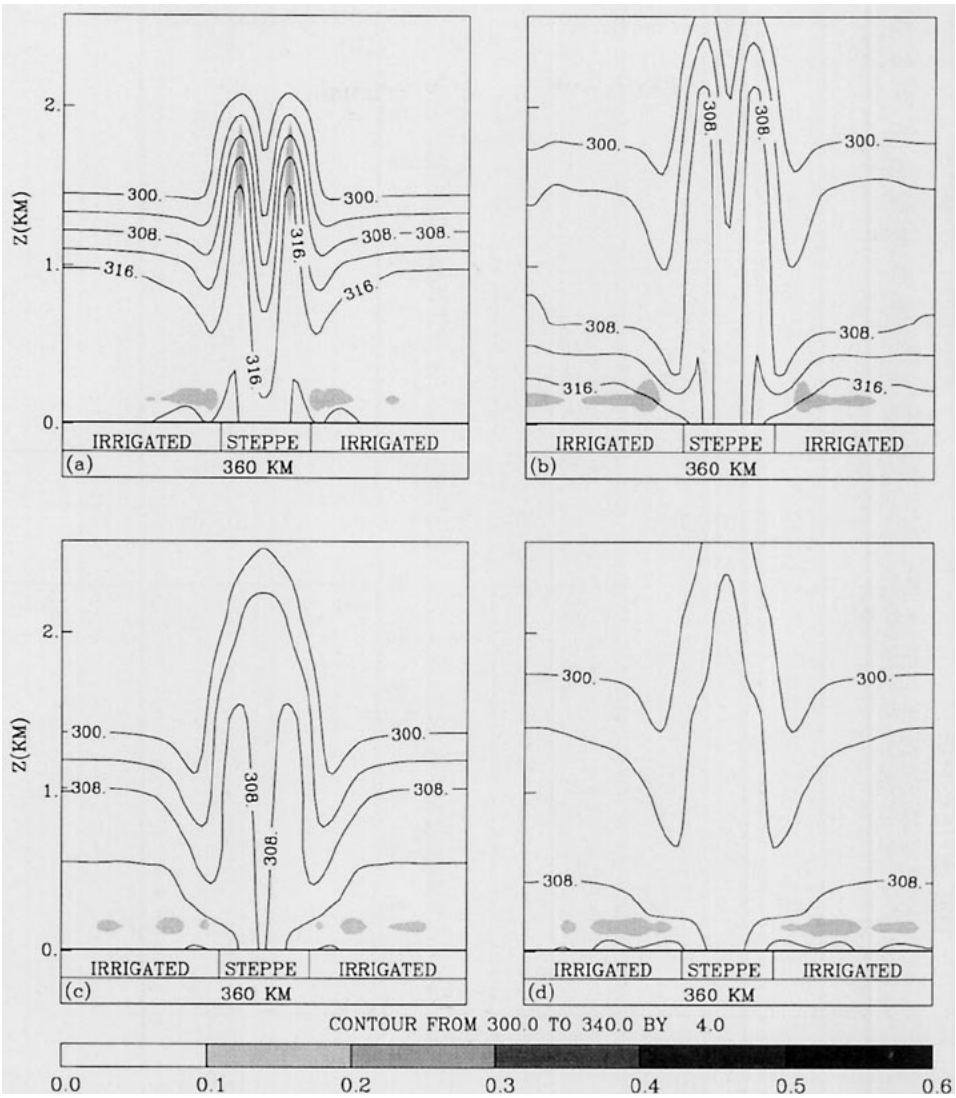

FIG. 4. The equivalent potential temperature θ_e (K) contours are overlaid on cloud water q_c (g kg^{-1}) for case 1: (a) absolutely stable, (b) conditionally unstable, (c) neutral boundary layer with an absolutely stable layer aloft, and (d) neutral boundary layer with a conditionally unstable layer aloft. The initial moisture in all cases was 90% relative humidity in the boundary layer with dry conditions aloft. The gray-scale bar at the bottom indicates the range and shading values for the cloud water.

concentrated. Figure 5c is the variation of domain TKE_{max} as a function of time. The results here are consistent with the cloud values. Initially, greater values of TKE_{max} exist for the neutral cases, where turbulence is not suppressed by the stability. The growth rate and largest values of TKE_{max} are generally greater for the neutral case with a conditionally unstable layer above. This situation represents the least stability and therefore the least suppression of existing turbulence. The oscillation in the TKE_{max} for the less stable cases results from the interaction of turbulence with cloud generation and solar radiation at the surface. However, this needs to be further investigated. The W_{max} shown in Fig. 5d corresponds to the TKE_{max}, with the W_{max} normally occurring after the corresponding TKE_{max}.

b. The influence of low-level moisture on clouds triggered by vegetation forcing (case 2)

A requirement to generate daytime convective clouds is the availability of adequate moisture, at least in the lower levels as shown in the results above. The potential for gravitational instability is related to the vertical stratification of water vapor in addition to the temperature stratification. When a moist layer exists near the surface with dry air aloft, the equivalent potential temperature θ_e decreases with height (i.e., $d\theta_e/dz < 0$). Forced lifting to saturation makes the layer unstable and produces moist convection. Moisture can be imported from great distances by large-scale wind systems, or it can be injected into the atmosphere by

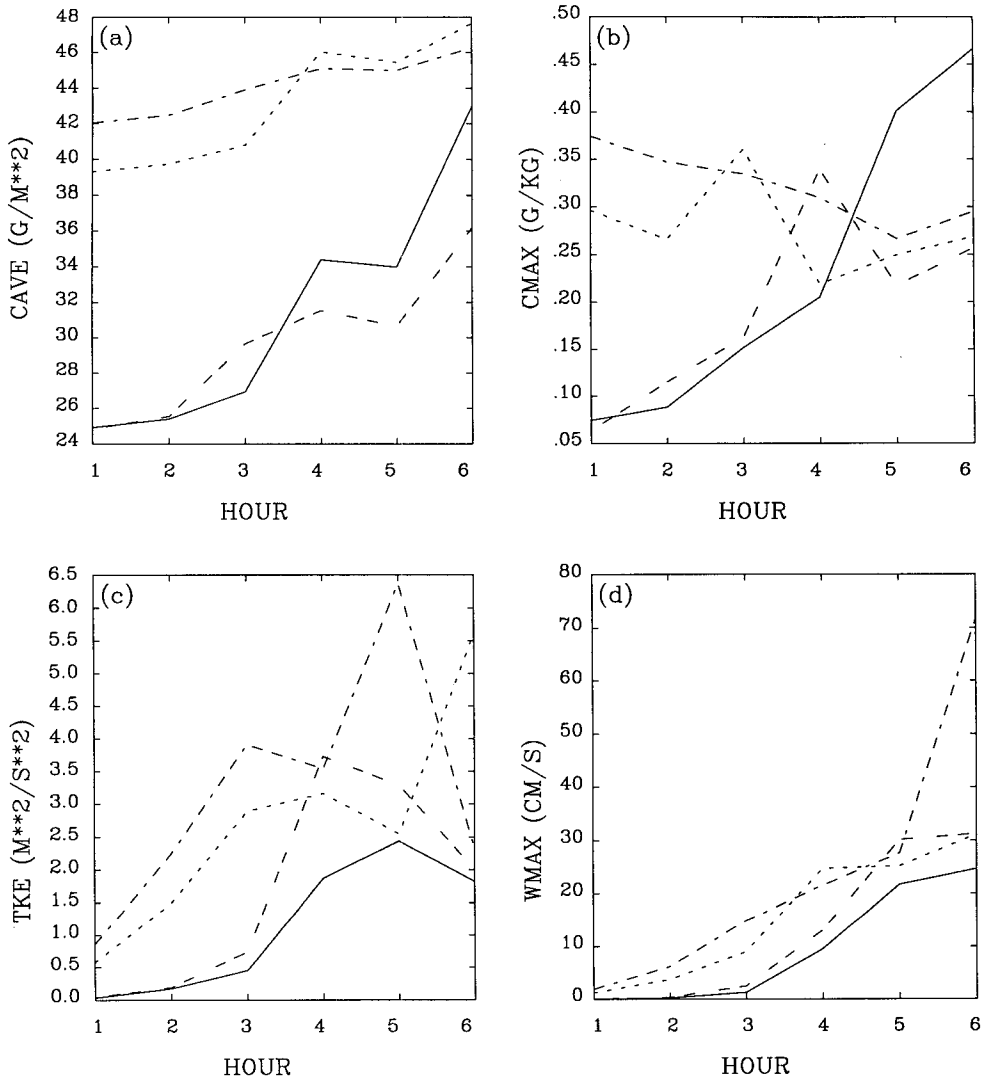

FIG. 5. (a) Integrated cloud water value, (b) maximum cloud water, (c) maximum TKE, and (d) maximum vertical velocity for the case 1. The solid line is for the absolutely stable case, the long-dashed line is for the conditionally unstable case, the dashed line is for a neutral boundary layer case with a stable layer aloft, and the alternating dashed–dot line is for a neutral boundary layer with a conditionally unstable layer aloft.

evaporation from local sources. The sensitivity of deep convection to moisture is very evident in drier regions. Even in cases where moisture from a large-scale source is inadequate, evaporation from local sources, such as lakes, marshes, or even regions where it has recently rained, can provide sufficient moisture for developing convective motion. The present study assumes that preexisting moisture could come from any source, including vegetation evapotranspiration. Formation of clouds with different moisture contents in the atmosphere by thermally induced mesoscale circulation as a triggering mechanism is then studied.

The model was initialized with an absolutely stable temperature profile, but by varying the initial relative humidity from 50% to 70%, 80%, and 100% and by limiting them to the lowest 1 km. Here only results from 80% and 100% are shown because the results from 50%, 70%, and 80% are similar. The distribution of vertical velocity and turbulence kinetic energy are shown in Fig. 6. The moisture effect on the magnitude and structure of vertical motion is minimal for all cases except for the saturated one. Increased low-level moisture destabilizes the atmosphere somewhat as the θ_e increases at low levels, but it has only a marginal effect on the bimodal updraft with a subsidence or a downdraft region between the two updrafts. The deepest convective motion appears with 100% initial relative humidity as the introduction of saturated moisture brings maximum moist static energy into the layer. A preexisting absolutely stable environment is not fa-

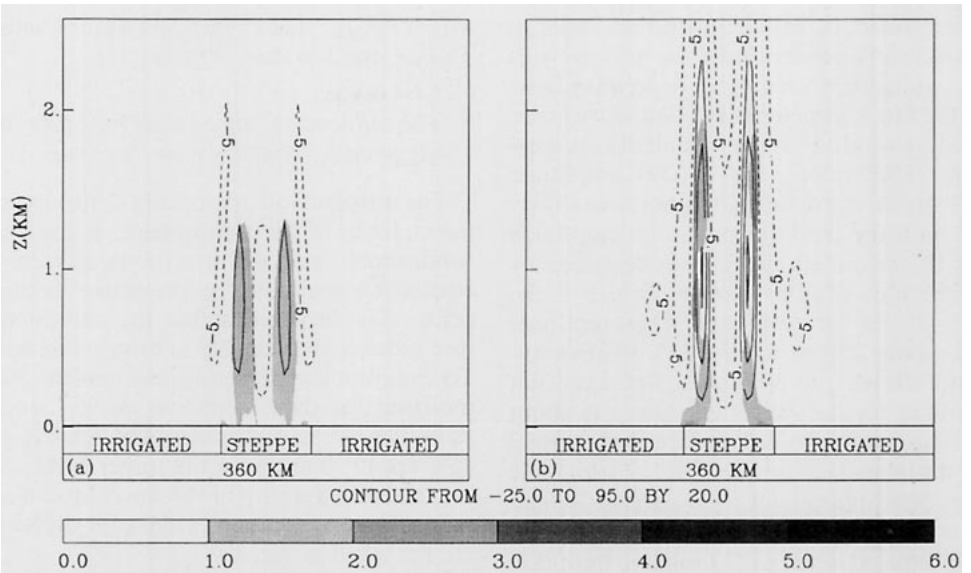

FIG. 6. The vertical velocity w (cm s^{-1}) are overlaid on TKE (m^2 s^{-2}) for case 2: (a) 80% and (b) 100% relative humidity, with the initial absolutely stable temperature profile. The gray-scale bar at the bottom indicates the range and shading values for the TKE.

vorable for the cell merger, as the stability damps the magnitude of the vertical motion and horizontal convergence. Strong surface heating inhomogeneities produce thermal circulations and destabilize the absolutely stable layer independent of the moisture content. However, the intensity of the subsequent circulation is significantly related to moisture content in the layer.

Contours of θ_e in Fig. 7 are overlaid on cloud water gray-scale patterns for case 2. The effect of moisture on the stability is evident by comparing the lapse rates of θ_e in Figs. 7a and 7b. In the least moist case, the lapse rate near 1 km is approximately 0.02 K m^{-1}. As moisture is added, the lapse rate of θ_e decreases (0.03 K m^{-1}, 0.04 K m^{-1}, to 0.05 K m^{-1} for the initial relative humidity of 70%, 80%, and 100%, respectively). All cases had the same initial surface temperature (θ = 291 K). Increased moisture (or latent heat) leads to increased θ_e. The exponential nature of the variation

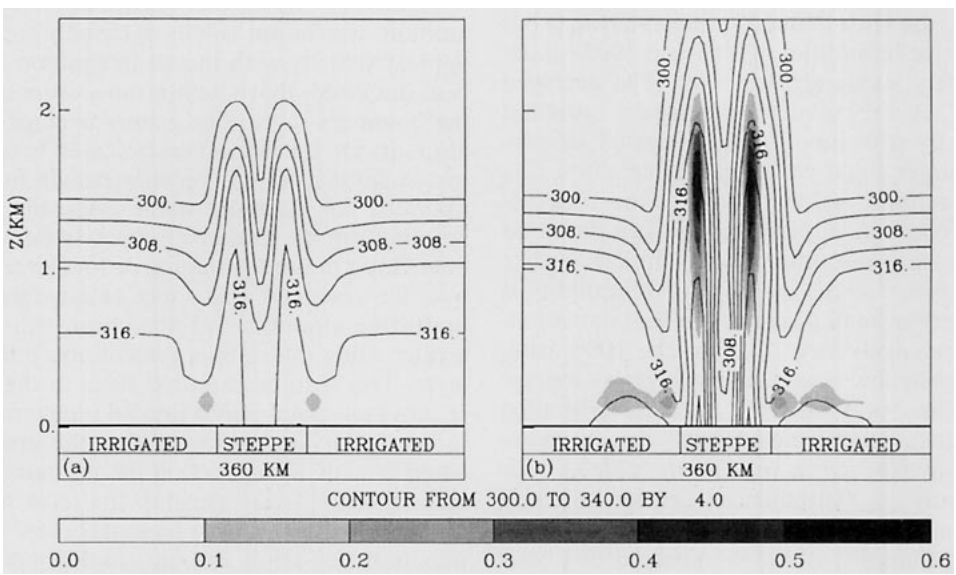

FIG. 7. The equivalent potential temperature θ_e (K) contours are overlaid on cloud water q_c (g kg^{-1}) for case 2: (a) 80% and (b) 100% relative humidity, with initial absolutely stable temperature profile. The gray-scale bar at the bottom indicates the range and shading values for the cloud water.

of the saturated moisture with temperature leads to much greater moisture content near the surface with larger θ_e values, and in turn creates more negative lapse rates through the first kilometer of the boundary layer. Increased moisture produces more turbulence, as is evident with larger TKE values (Fig. 6). The amplitude of the convectively driven disturbance increases slowly with increased moisture until the maximum amplitude is realized for the saturated air. This is best seen by focusing on the value of 300 K for θ_e, which is the lowest contour drawn for each case. The amplitude increases from about 200 m for the 50% relative humidity case (not shown), to 300 m for 70% case (not shown), to 350 m for the 80% case, but it is about 1000 m for the saturated case. Again, increased thermal forcing due to the latent heat release leads to a dramatic increase in vertical displacement of air parcels. In reality, such conditions could lead to deep convection.

Clouds are produced when initial relative humidity is above 90% (Fig. 4a and Fig. 7b). More cloud water and a deeper cloud layer appeared for the 100% initial relative humidity, indicating that a more moist environment is more conducive to the formation of moist convection through the increase of low-level moist static energy. The stable stratification supports a gradual buildup of a large amount of moist static energy within the boundary layer. The feedback of cloud formation on the updraft/downdraft is evident in the velocity components. The enhanced buoyancy due to latent heating develops stronger circulation, with larger vertical velocities than in the unsaturated atmosphere. More fog forms over the vegetated area as the initial relative humidity is increased (Fig. 7). The cloud water content in the fog also increases with increased initial moisture content, as expected.

Figure 8 has the same defined variables as Fig. 5 but for initial relative humidities of 80% and 100% under initial absolutely stable environment. The averaged cloud water C_{ave} is very small for relative dry cases and increases slightly with time. Initial saturated air produces much larger cloud water than other cases; C_{ave} reaches its maximum value at hour 5 and then decreases as the convective motion evaporates the cloud water. Maximum cloud water C_{max} is similar to C_{ave}. The value increases as the initial relative humidity is increased. There is small C_{max} early in the simulation, even for the relatively large C_{ave} for the 100% case, indicating the shallow condensation layer as fog appears. Maximum cloud water C_{max} increases with time for all cases, including for the relatively dry initial environment; C_{max} reached its maximum value at hour 5 consistent with C_{ave}. Turbulence increases with both time and initial relative humidity. The TKE_{max} for the initial relative humidity of 100% appeared one hour earlier than C_{ave} and C_{max}, indicating the cloud water to be maximum after the strongest turbulence is produced. Vertical velocity W_{max} values are also consistent with TKE_{max}. They reach maximum values 1 h after TKE_{max} reaches its maximum.

c. *The influence of upper-level moisture on clouds triggered by vegetation forcing (case 3)*

The introduction of moisture in the upper layer alters the stability of the atmosphere. If the upper layer is conditionally unstable and moist, a thermally induced circulation could trigger convective motion. If the upper level is absolutely stable, the introduction of moisture reduces the stability (Durran and Klemp 1982). To examine the triggering mechanism of upper-layer moisture for the convective motion under different stabilities, we assume an initial relative humidity of 45% rather than 0% in the upper layer. As in case 1, the relative humidity of the lower level is still 90% initially. The temperature profiles for different stabilities are the same as Fig. 1.

The introduction of moisture in the atmosphere above the boundary layer increases cloud water and has greatest effect on lapse rate of θ_e in that layer, as shown on Figs. 9 and 10, which depict the TKE and vertical velocity contours and the cloud water and θ_e, respectively, for the same stability categories as Fig. 1. It is obvious by comparing the θ_e values in Fig. 10 to those in Fig. 4 for the drier case (case 1) that the maximum change is in the upper levels. The lapse rate of θ_e is much less for the more moist case shown in Fig. 10 than the drier case in Fig. 4. The moisture increases the buoyancy and therefore destabilizes the atmosphere, leading to larger cloud water amounts than the drier case (case 1). Otherwise, few differences are apparent when moisture is added to the layer above the boundary layer.

Figure 11 shows the variation of average cloud amount, maximum values of cloud water, TKE, and vertical velocity with model integration hour for the case discussed above with a moist atmosphere above the boundary layer. The greater average cloud water amounts for the neutral cases (cases 3c and 4d) early in the simulation are because clouds formed in the updrafts. For the more stable cases, the initial cloud amounts are the same with cases 1a and 1d since the only cloud present is the fog or low-level cloud water over the vegetated area. Once clouds form in the updrafts, the amounts and maximum values are much greater when moisture is present above the boundary layer. This is to be expected since in the dry-air case (case 1) the cloud builds into an unfavorable environment and dry air entrained into the updraft inhibits cloud growth. The effect on the updraft speed can be seen in Fig. 11d. In general, the local maximum of vertical velocity coincides reasonably well with the local maximum of cloud amounts and cloud water maximum values. Also, the maximum vertical velocities are in general greater than corresponding maxima in the cases with dry air aloft (shown in Fig. 5d). The

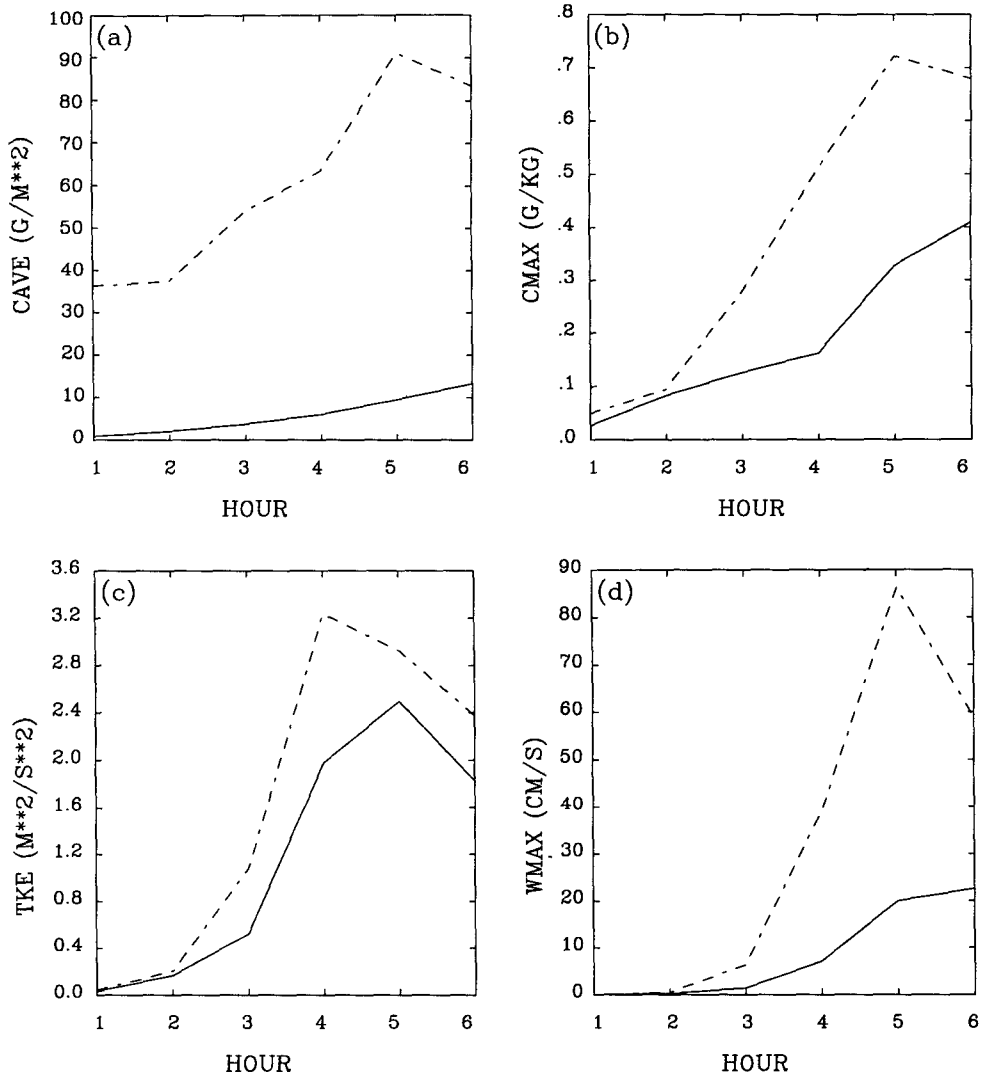

FIG. 8. (a) Integrated cloud water value, (b) maximum cloud water, (c) maximum TKE, and (d) maximum vertical velocity for case 2. The relative humidity is 80% (solid line) and 100% (alternating dash-dot line).

additional latent heat release in the present case creates additional buoyancy, which in turn drives the stronger updrafts. As in the earlier case, the vertical velocity maximums lag the TKE maximum by about 1 h.

d. The effects of horizontal heating scales on vegetation forcing of clouds (case 4)

Anthes (1984) estimated the preferred horizontal scale of the vegetation bands for producing moist convection using a linear model. For bands of width less than about 20 km, horizontal mixing limits the vertical penetration of the surface heating perturbation to heights too small to be effective in generating moist convection. For large scales (widths of about 100 km), however, it appears that vertical circulations can extend to heights of 1 km or more, which is capable of initiating and enhancing moist convection when combined with increases in low-level moist static energy.

To study the effect, four simulations with different horizontal scales (20, 40, 80, 120 km) of surface heating were run using the numerical model. The idealized sounding data used here are shown in Fig. 12. The temperature lapse rate is the same as the one for the absolutely stable cases discussed above. High moisture content in the relative humidity profile indicates strong potential instability up to 5 km. This initial condition is favorable in developing convective motion when a sufficient trigger mechanism is provided through different horizontal heating scales.

Surface convergence and updraft motion are strong when the horizontal heating scale is narrow (Figs. 13a and 13b). A large contrast of properties of the atmosphere over vegetated areas and bare soil areas builds

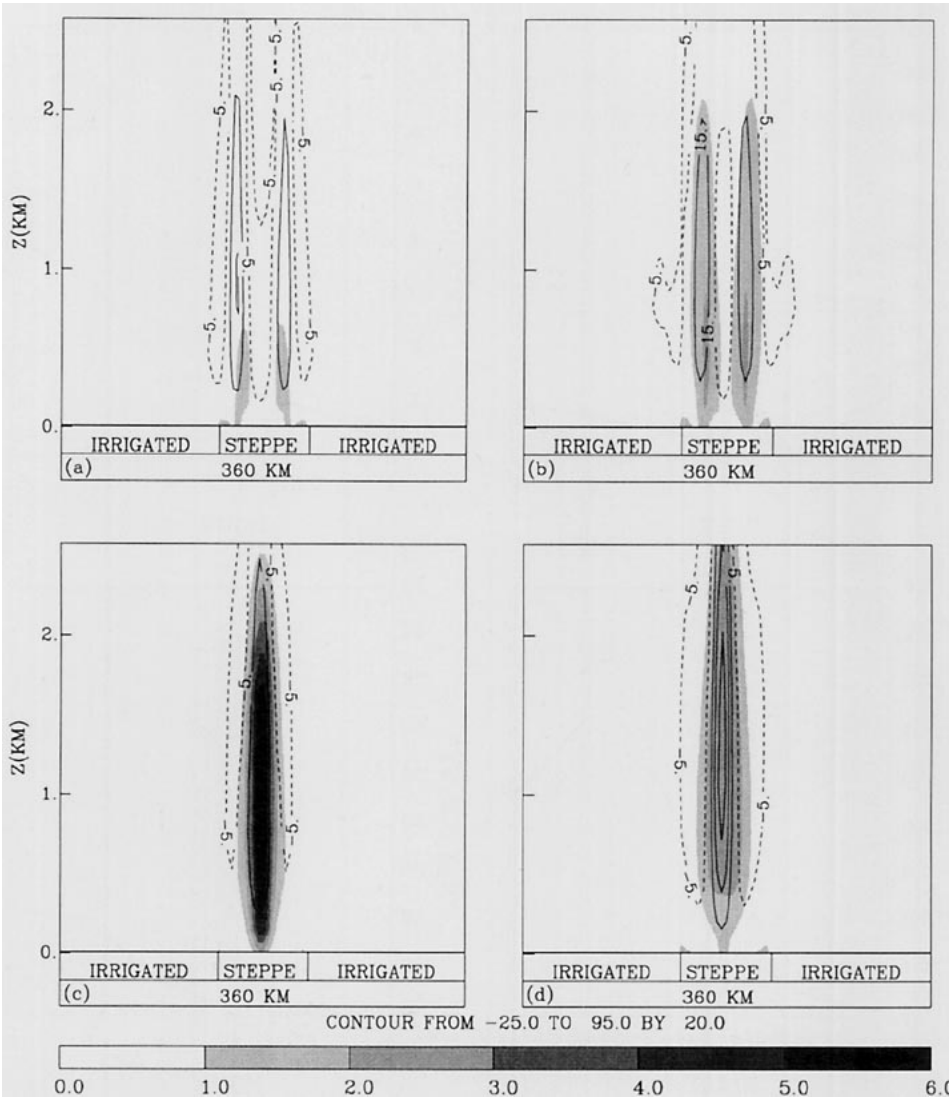

FIG. 9. The vertical velocity w (cm s^{-1}) are overlaid on TKE (m^2 s^{-2}) for case 3: (a) absolutely stable, (b) conditionally unstable, (c) neutral boundary layer with an absolutely stable layer aloft, and (d) neutral boundary layer with a conditionally unstable layer aloft. The initial moisture in all cases was 90% relative humidity in the boundary layer with 45% relative humidity in the atmosphere above the boundary layer. The gray-scale bar at the bottom indicates the range and shading values for the TKE.

strong horizontal gradients of heat fluxes. This destabilizes the initial absolutely stable stratified atmosphere significantly. Only one circulation cell is produced by the narrow horizontal heating scale (Fig. 13a). When the horizontal heating scale is increased (Fig. 13b), the contrast of atmospheric properties between vegetated areas and bare soil areas decreases. This leads to a decrease in the horizontal gradient of heat fluxes. The intensity of thermally induced circulation is weaker as compared to the narrow-horizontal-scale case. When the horizontal scale is increased further, the horizontal gradient of heat fluxes have large values only near the interfaces between vegetated areas and bare soil areas. Two thermally induced circulation cells are produced. The effects of increasing the horizontal scale to 80 and 120 km are shown in Figs. 13c and 13d, respectively. When the horizontal separation between the two circulation cells increases, the surface convergence and vertical motion in each cell increases. This is due to weaker interaction between the two cells for the larger horizontal scales. The height of turbulent mixing increases as the horizontal heating scale increases because the vertical penetration of the surface heating perturbation is stronger for larger horizontal scale.

Clouds are generated for all four cases with the initially favorable environments since a strong thermally induced updraft motion occurs with all four different horizontal heating scales. The clouds are produced fol-

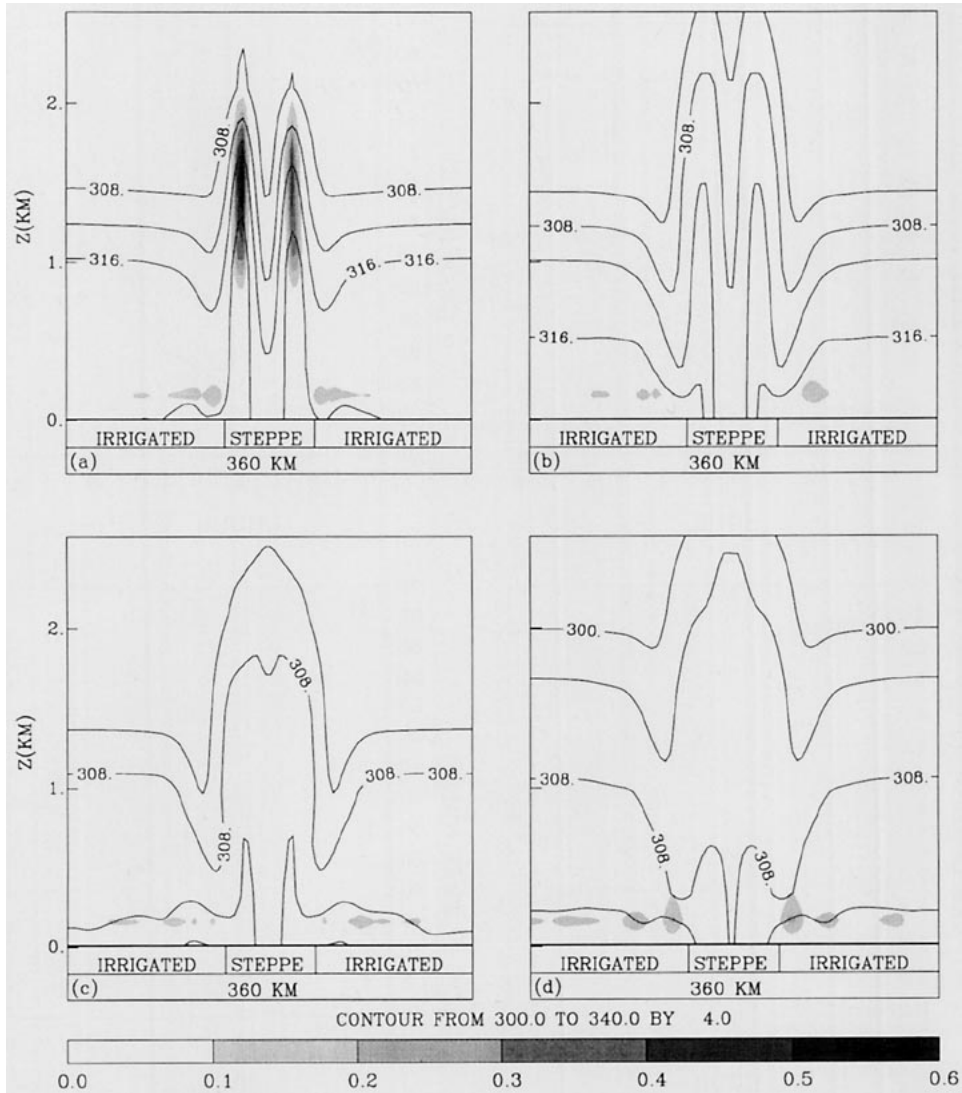

FIG. 10. The equivalent potential temperature θ_e (K) contours are overlaid on cloud water q_c (g kg^{-1}) for case 3: (a) absolutely stable, (b) conditionally unstable, (c) neutral boundary layer with an absolutely stable layer aloft, and (d) neutral boundary layer with a conditionally unstable layer aloft. The initial moisture in all cases was 90% relative humidity in the boundary layer with 45% relative humidity in the atmosphere above the boundary layer. The gray-scale bar at the bottom indicates the range and shading values for the cloud water.

lowing the updraft branch; therefore, the cloud cells are consistent with the circulation cells. There is only one cloud cell when horizontal scales are less than 40 km. However, more cloud water appears for larger horizontal heating scales. More low-level clouds in the narrowest case (Fig. 14a) indicates that vegetation evapotranspiration is more important with smaller-scale horizontal heating. The moist static energy is large and similar for all the four cases because the initial environments are the same, as shown in Fig. 14. The potential instability is slightly stronger in the cloud layer for the case of the smallest horizontal heating scale, which is consistent with the smaller value of cloud water.

Average cloud amount and maximum value of cloud water, TKE, and vertical velocity for the cases discussed above with different horizontal heating scales (20, 40, 80, and 120 km, respectively) are shown in Figs. 13a, 13b, 13c, and 13d. About the same small amount of average cloud water appeared in the early hours (Fig. 15a) of model integration, implying that the condensation of water vapor is independent of the horizontal heating scales because the horizontal gradient of heat fluxes is not yet dominant. The average cloud water increases with time, and differences between the different horizontal scales begin to appear. The smallest horizontal heating-scale case produces the largest amount of average cloud water. The average cloud wa-

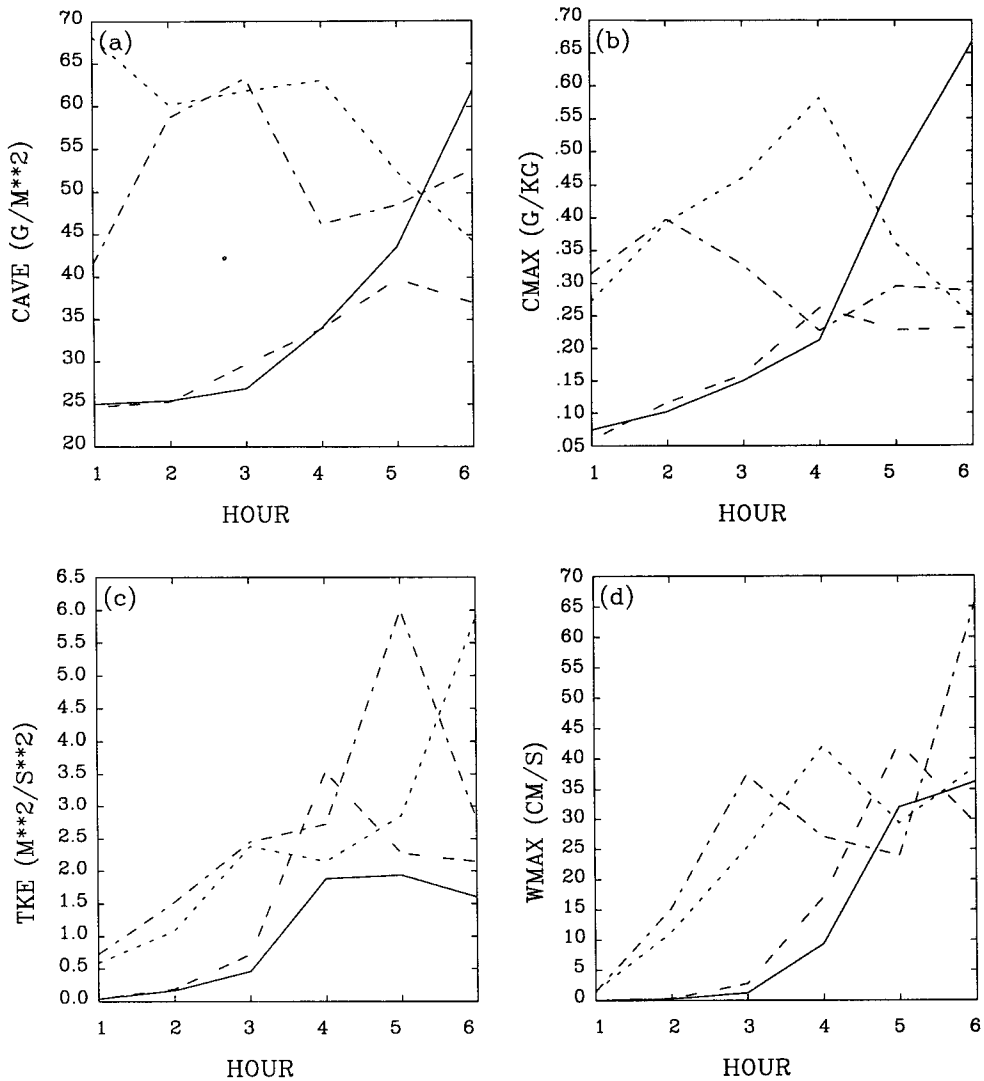

FIG. 11. (a) Integrated cloud water value, (b) maximum cloud water, (c) maximum TKE, and (d) maximum vertical velocity for case 3. The solid line is for the absolutely stable case, the long-dashed line is for the conditionally unstable case, the dashed line is for a neutral boundary layer case with a stable layer aloft, and the alternating dash–dot line is for a neutral boundary layer with a conditionally unstable layer aloft.

ter reaches a maximum value faster than other cases. The smallest amount of average cloud water is for the case with 40-km horizontal heating scale. The average cloud water for the other two larger horizontal scales has a similar increasing tendency. Their amounts are larger than the case with 40-km horizontal heating scale and smaller than the case with 10-km horizontal heating scale.

Variation of the maximum cloud water is shown in Fig. 15b. The tendency for the maximum cloud water is similar to that of average cloud water for all horizontal heating scales. The maximum cloud water is largest for 20-km horizontal heating-scale case and is the smallest for 40-km horizontal heating-scale case. Other two cases have the maximum cloud water between the largest and smallest cases. The tendency of maximum cloud water for these two cases are slightly different from the average cloud water. The tendency of maximum TKE and vertical velocity are similar to that of the cloud water discussed above. The maximum TKE corresponds to the maximum average cloud water and the maximum cloud water.

The results indicate that convective cells formed by differential surface heating not only relate to the horizontal heating scale but also large-scale conditions, as proposed in the Anthes hypothesis (1984). A very moist initial atmosphere in the present simulation generates convective clouds for a horizontal heating scale narrower than that proposed by Anthes (1984) and Yan and Anthes (1988). The interaction of the

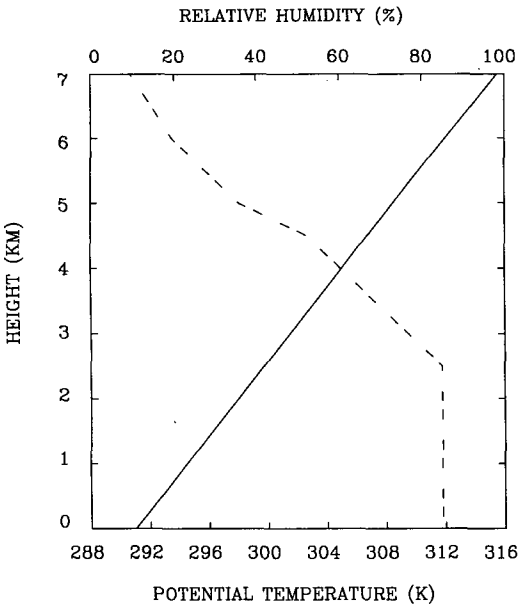

FIG. 12. The initial potential temperature and relative humidity profiles for case 4 investigating the effect of horizontal scale of vegetation forcing. The potential temperature is labeled on the bottom axis, the relative humidity on the top axis. Height is labeled on the left.

large-scale conditions and the scale of horizontal surface heating for convective cloud formation also can be seen in case 1, where the effects of different atmospheric stability on cloud formation were investigated. Two convective cells are generated early in the simulation and merge into one cell with the initially neutral atmosphere (Figs. 3c and 3d). This results agree with those of Yan and Anthes (1988). When large-scale conditions change (case 4) to stable atmosphere, two convective cells persist rather than merge. Results from the experiments also show that merging of the two cells is sensitive to atmospheric stability but not moisture content.

5. Summary and conclusions

A two-dimensional PBL numerical model with an explicit cloud physics and a comprehensive vegetation parameterization scheme has been used to demonstrate the effectiveness of vegetation as a surface forcing to trigger cloud formation under different atmospheric environments. These included the variations in the atmospheric stability and the atmospheric moisture content in the planetary boundary layer and the layer above it. Numerical experiments also investigated the effect of the horizontal length scale of the surface forcing on triggering convective clouds.

The effects of atmospheric stability were investigated by using three different stability regimes in the lower atmosphere: absolutely stable, conditionally unstable, and neutral with a dry layer above the boundary layer. The effects of moisture were investigated by initializing the model with different moisture profiles with the same static stability. Moisture was added in the upper layer for the three stability regimes to investigate the effect of deep moisture layer. And finally, the effects of horizontal length scales on the surface forcing were studied by altering the length of the steppe region between two irrigated regions.

In the simulation of different atmospheric stabilities with 90% relative humidity in the lower layer and 0% relative humidity in the layer above, the results indicate that vegetation as a surface forcing triggers convective clouds but is very sensitive to the background atmospheric conditions. The magnitude of the vertical component is less for the more stable case since greater stability, and therefore greater restoring force, leads to smaller amplitude buoyancy-generated disturbances. Two convective cells form in response to thermal circulations that develop at both interfaces between the vegetation and the bare soil. In the weaker stability cases, the smaller restoring force allows the two cells to merge into one updraft, which is consistent with the results of Yan and Anthes (1988). The results also show that the atmospheric stability can affect the growth and the merger of these convective cells. However, clouds persist longer only for the initially stable environment because the stable stratification supports a gradual buildup of a large amount of moist static energy within the boundary layer and less vertical mixing into the drier air aloft. Formation of clouds earlier for less stable condition is attributable to the earlier existence of turbulence. Eventually the clouds dissipate in the weaker stability cases as the cloud water is ventilated into the drier atmosphere aloft.

Numerical experiments with atmospheric moisture contents of 50%, 70%, 80%, and 100% relative humidity in the boundary layer are conducted to investigate the vegetation forcing in the formation of convective clouds under initially absolutely stable atmospheric environment. The results show that lower-layer atmospheric moisture content is very important to the vegetation triggering mechanism. With the initial absolutely stable environment, the intensity of the thermally induced circulation is directly related to the moisture content since increased low-level moisture increases the potential instability. Two cells form for all atmospheric moisture contents used in this study. Clouds are generated when the initial relative humidity is above 90% since a moister environment is more conducive to the formation of clouds through an increase in the low-level moist static energy. The amplitude of the convectively driven disturbance increases with increased moisture

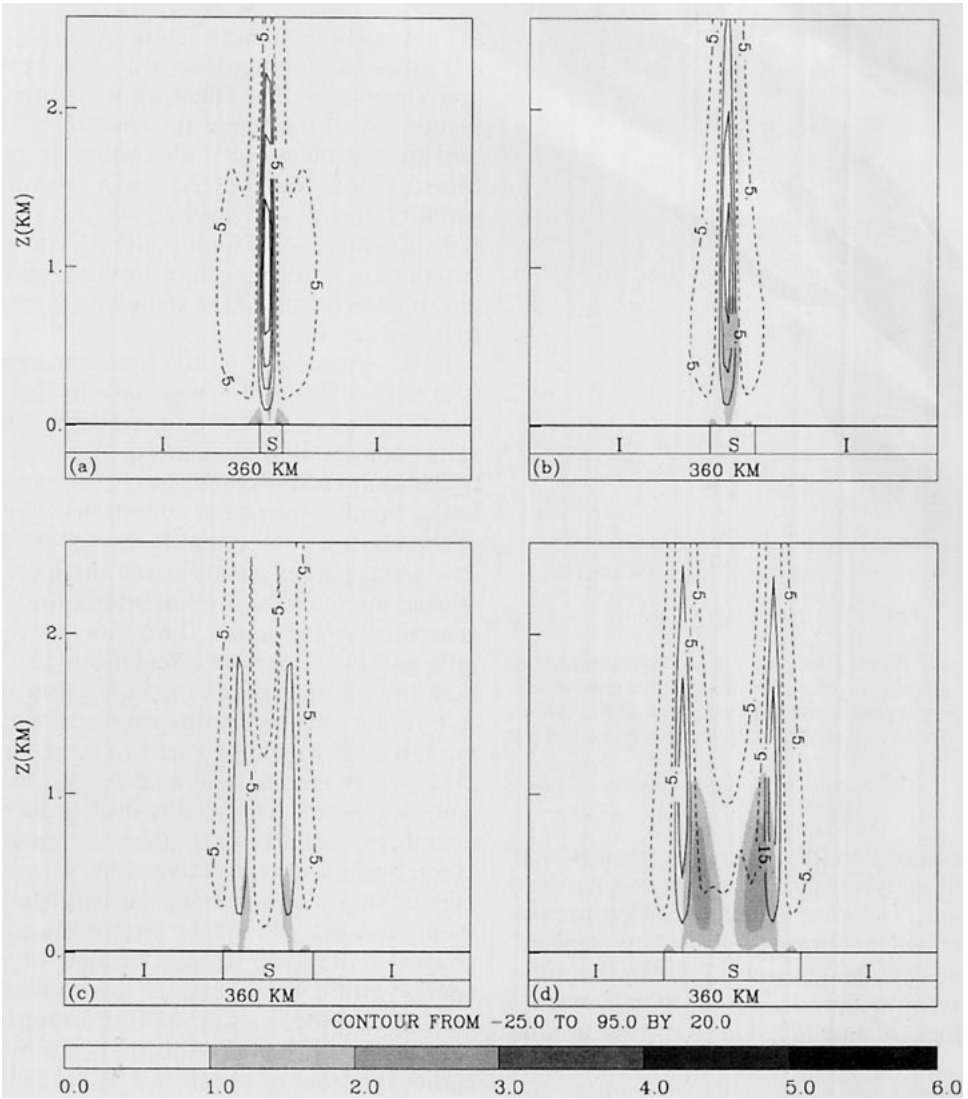

FIG. 13. The vertical velocity w (cm s^{-1}) are overlaid on TKE (m^2 s^{-2}) for case 4. A steppe area (labeled S) was placed between two irrigated (I) areas. The steppe was varied from (a) 20, (b) 40, (c) 80, to (d) 120 km. The gray-scale bar at the bottom indicates the range and shading values for the cloud water.

as turbulence and low-level moist static energy increase.

The introduction of moisture in the atmosphere above the boundary layer modifies the atmosphere by changing the potential instability. Under this more favorable atmospheric condition, vegetation forcing produces more cloud water for initial absolutely stable case. The amplitudes of the disturbances are larger with more moisture present. Few differences are apparent for other stability conditions. Clouds form early in the simulations for the neutral cases but dissipate later. Average cloud amounts are similar between cases with dry and moist upper layer.

Different horizontal heating scales produce different convective cells under the same initial condition. One convective cell is generated for a narrow horizontal heating scale and two convective cells for wider horizontal heating scales. The interaction between two convective cells is related to horizontal heating scales. The amount of cloud water present reflects the magnitude of the vertical velocity, except for the most narrow horizontal steppe where the maximum cloud water and total cloud amounts preceded the maximum values of vertical velocity. The depth of turbulent mixing increases as the horizontal heating scale increases due to the greater surface heating over a larger horizontal area. When horizontal heating scale becomes small, the increased evaportranspiration due to increased vegetated areas might increase surface-layer fog or cloud water.

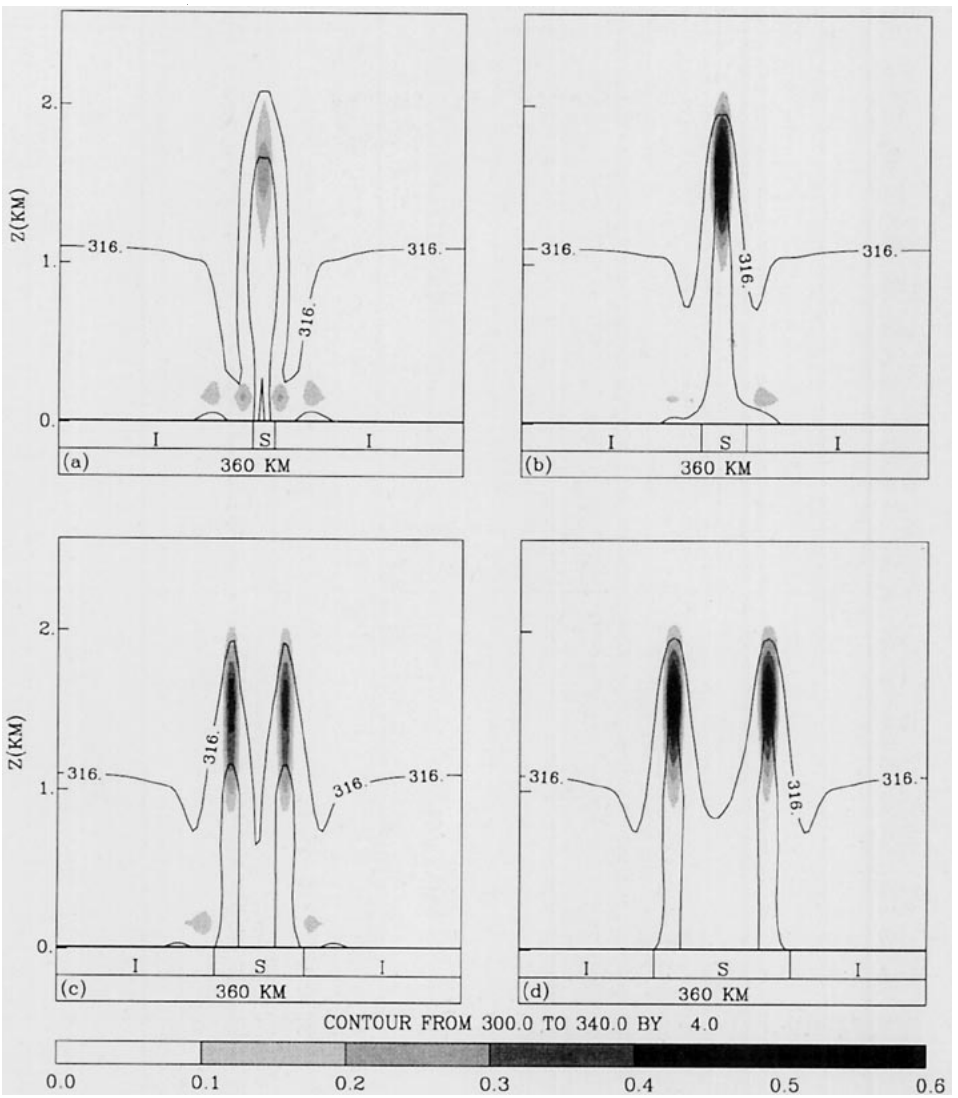

FIG. 14. The equivalent potential temperature θ_e (K) contours are overlaid on cloud water q_c (g kg^{-1}) for case 4. A steppe area (labeled S) was placed between two irrigated (I) areas. The steppe was varied from (a) 20, (b) 40, (c) 80, to (d) 120 km. The gray-scale bar at the bottom indicates the range and shading values for the TKE.

The results indicate that convective cells formed by differential surface heating not only depends on the horizontal heating scale but also on large-scale conditions, as suggested by Anthes (1984). The very moist atmospheric condition in the present simulation leads to convective clouds for horizontal heating scale narrower than that proposed by Anthes (1984) and Yan and Anthes (1988).

Acknowledgments. This work was supported by the U.S. Department of Energy and by the National Science Foundation. The majority of the computations were performed at the National Supercomputer Center for Energy and the Environment. Additional computer time was provided by the DOE at the National Energy Research Supercomputer Center and by the North Carolina Supercomputing Center.

APPENDIX

Model Equations

The governing equations of the mean flow, in which the liquid water is separated into cloud water and rainwater, are expressed in the terrain-following coordinate σ as follows:

$$\frac{\partial u}{\partial t} = -u\frac{\partial u}{\partial x} - \dot{\sigma}\frac{\partial u}{\partial \sigma} + fv - \theta_v\frac{\partial \pi}{\partial x} - g(1-\sigma)\frac{\partial \hat{E}}{\partial x} + \frac{\partial}{\partial x}\left(K_H\frac{\partial u}{\partial x}\right) + \frac{1}{H-\hat{E}}\frac{\partial}{\partial \sigma}(\overline{-u'w'}), \quad \text{(A1)}$$

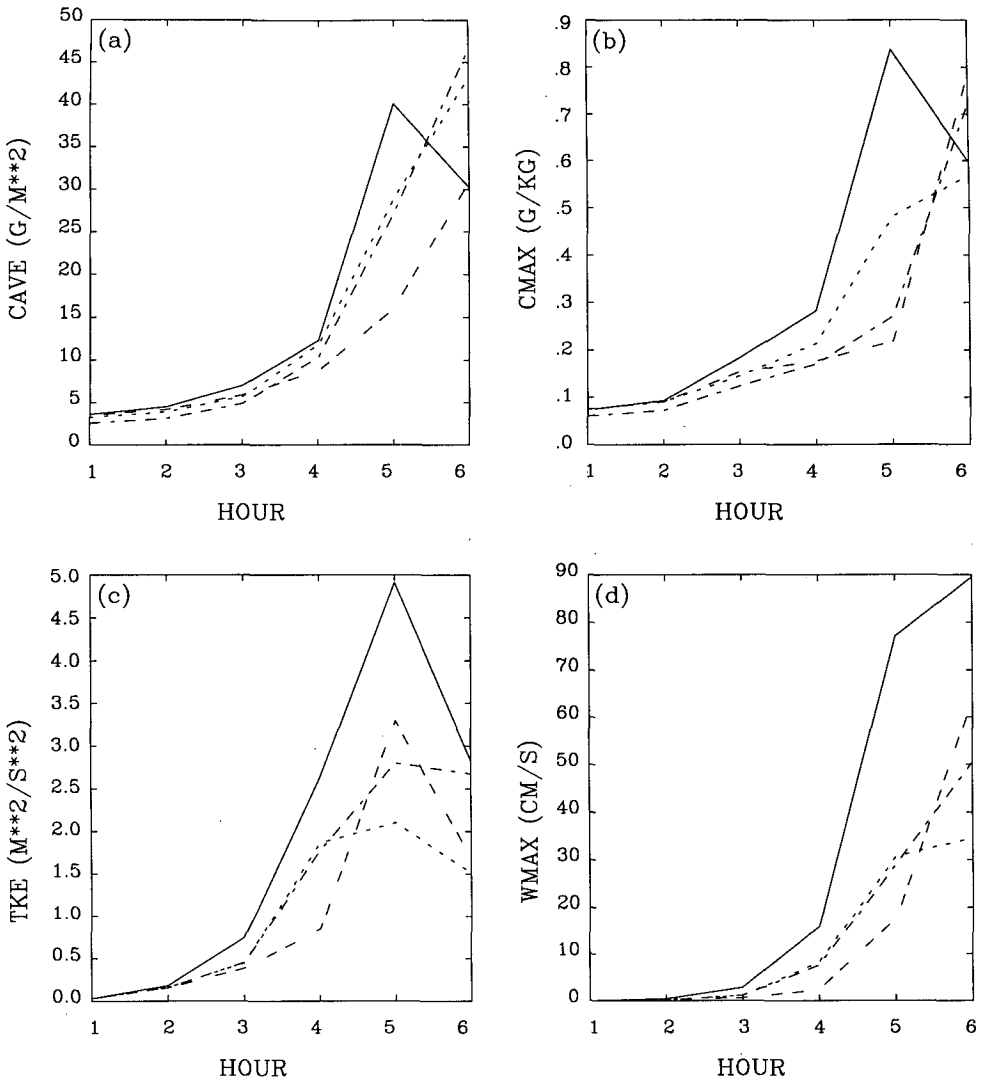

FIG. 15. (a) Integrated cloud water value, (b) maximum cloud water, (c) maximum TKE, and (d) maximum vertical velocity for case 4. The steppe area was varied from 20 (solid line), 40 (long-dashed line), 80 (dashed line), to 120 km (alternating dash–dot line).

$$\frac{\partial v}{\partial t} = -u\frac{\partial v}{\partial x} - \dot{\sigma}\frac{\partial v}{\partial \sigma} - fu + \frac{\partial}{\partial x}\left(K_H\frac{\partial v}{\partial x}\right) + \frac{1}{H-\hat{E}}\frac{\partial}{\partial \sigma}(\overline{-v'w'}), \quad \text{(A2)}$$

$$\frac{\partial \theta}{\partial t} = -u\frac{\partial \theta}{\partial x} - \dot{\sigma}\frac{\partial \theta}{\partial \sigma} + \frac{\partial}{\partial x}\left(K_H\frac{\partial \theta}{\partial x}\right) + \frac{1}{H-\hat{E}}\frac{\partial}{\partial \sigma}(\overline{-w'\theta'}) + S_\theta, \quad \text{(A3)}$$

$$\frac{\partial q_j}{\partial t} = -u\frac{\partial q_j}{\partial x} - \dot{\sigma}\frac{\partial q_j}{\partial \sigma} + \frac{\partial}{\partial x}\left(K_H\frac{\partial q_j}{\partial x}\right) + \frac{1}{H-\hat{E}}\frac{\partial}{\partial \sigma}(\overline{-w'q_j'}) + S_j + R_j, \quad \text{(A4)}$$

$$\frac{\partial \rho u(H-\hat{E})}{\partial x} + \frac{\partial \rho\dot{\sigma}(H-\hat{E})}{\partial \sigma} = 0, \quad \text{(A5)}$$

$$\frac{\partial \pi}{\partial \sigma} = -\frac{g(H-\hat{E})}{\theta_v}. \quad \text{(A6)}$$

Equations (A1) and (A2) are horizontal momentum equations for east–west velocity u and north–south velocity v. Equation (A3) is the thermodynamic equation for the potential temperature θ. Equation (A4) represents mass conservation of water for phase category j. The five category scheme includes water vapor q, cloud water q_c, rainwater q_r, cloud ice q_i, and snow q_s. The S_j and R_j represent transfer (sources and sinks) between any two phase categories and removal of water by precipitation processes, respec-

tively. Equation (A5) is the anelastic equation for mass continuity. Equation (A6) is the hydrostatic equation. The above model equations assume that the flow is hydrostatic in the terrain-following coordinate σ defined as

$$\sigma = \frac{z - \hat{E}}{H - \hat{E}}, \tag{A7}$$

where H is total height considered in the model and $\hat{E}$ is terrain height. The anelastic approximation is used to suppress generation of unwanted and meteorologically insignificant sound waves (Pielke 1984). The elimination of these fast-moving waves allows the use of a larger time step for integration. The vertical velocity in σ coordinate ($\dot{\sigma}$) is related to vertical velocity in z coordinate (w) in the anelastic equation for fluid continuity as follows:

$$w = \dot{\sigma}(H - \hat{E}) - (\sigma - 1)\left(u\frac{\partial \hat{E}}{\partial x}\right). \tag{A8}$$

The scaled pressure and the virtual potential temperature are defined, respectively, as follows:

$$\pi = C_p\left(\frac{p}{p_{00}}\right)^{\kappa}, \quad \kappa = \frac{R}{C_p} \tag{A9}$$

$$\theta_v = \theta(1 + 0.61\, q - q_c - q_r - q_i - q_s), \tag{A10}$$

where the reference pressure chosen as $P_{00} = 10^5$ Pa.

REFERENCES

Anthes, R. A., 1984: Enhancement of convective precipitation by mesoscale variations in vegetative covering in semiarid regions. *J. Climate Appl. Meteor.*, **23,** 541–554.

Avissar, R., and R. A. Pielke, 1989: A parameterization of heterogeneous land surface for atmospheric numerical models and its impact on regional meteorology. *Mon. Wea. Rev.*, **117,** 2113–2136.

——, and F. Chen, 1993: Development and analysis of prognostic equations for mesoscale kinetic energy and mesoscale (subgrid scale) fluxes for large-scale atmospheric models. *J. Atmos. Sci.*, **50,** 3751–3774.

Banta, R., 1990: The role of mountain flows in making clouds. *Atmospheric Processes over Complex Terrain, Meteor. Mongr.*, No. 23, Amer. Meteor. Soc., 229–323.

Bougeault, P., J. Noilhan, P. Lacarrère, and P. Mascart, 1991: An experiment with an advanced surface parameterization in a mesobeta-scale model. Part I: Implementation. *Mon. Wea. Rev.*, **119,** 2358–2373.

Boybeyi, Z., and S. Raman, 1992: A three-dimensional numerical sensitivity study of convection over the Florida peninsula. *Bound.-Layer Meteor.*, **60,** 325–359.

Businger, J. A., J. C. Wyngaard, Y. Izumi, and E. F. Bradley, 1971: Flux-profile relationships in the atmospheric surface layer. *J. Atmos. Sci.*, **28,** 181–189.

Deardorff, J. W., 1974: Three-dimensional numerical study of the height and mean structure of a heated planetary boundary layer. *Bound.-Layer Meteor.*, **7,** 81–106.

——, 1978: Efficient prediction of ground surface temperature and moisture, with inclusion of a layer of vegetation. *J. Geophys. Res.*, **20,** 1889–1903.

Doran, J. C., and Coauthors, 1992: The Boardman Regional Flux Experiment. *Bull. Amer. Meteor. Soc.*, **73,** 1785–1795.

Durran, D. R., and J. B. Klemp, 1982: The effects of moisture on trapped mountain lee waves. *J. Atmos. Sci.*, **39,** 2490–2506.

Houze, Jr., R. A., 1993: Cloud dynamics. *International Geophysics Series,* **53,** 262 pp.

Hong, X., 1993: A numerical modeling study of vegetation as a surface forcing for mesoscale circulation and cloud formation. M. S. thesis, North Carolina State University, Raleigh, 98 pp.

——, M. J. Leach, and S. Raman, 1994: Role of vegetation in generation of mesoscale circulation. *Atmos. Environ.*, **28,** in press.

Huang, C. Y., 1990: A mesoscale planetary boundary layer model for simulations of topographically induced circulations. Ph.D. dissertation. North Carolina State University, Raleigh, 253 pp.

——, and S. Raman, 1991a: Numerical simulation of January 28 cold air outbreak during GALE, part I: The model and sensitivity tests of turbulence closures. *Bound.-Layer Meteor.*, **55,** 381–407.

——, and ——, 1991b: Numerical simulation of January 28 cold air outbreak during GALE, part II: The mesoscale circulation and marine boundary layer. *Bound.-Layer Meteor.*, **56,** 51–81.

——, and ——, 1992: A three-dimensional numerical investigation of a Carolina coastal front and the Gulf Stream rainband. *J. Atmos. Sci.*, **49,** 7, 560–584.

Kasten, F., and G. Czeplak, 1980: Solar and terrestrial radiation dependent on the amount and type of cloud. *Solar Energy,* **24,** 177–189.

Klemp, J. B., and D. R. Durran, 1983: An upper boundary condition permitting internal gravity wave radiation in numerical mesoscale model. *Mon. Wea. Rev.*, **111,** 430–444.

Leach, M. J., 1994: The interactive role of clouds and radiative transfer in maintaining atmospheric circulation. Ph.D. dissertation. North Carolina State University, Raleigh, 150 pp.

Louis, J. F., 1979: A parametric model of vertical eddy fluxes in the atmosphere. *Bound.-Layer Meteor.*, **17,** 187–202.

Mahfouf, J.-F., E. Richard, and P. Mascart, 1987: The influence of soil and vegetation on the development of mesoscale circulations. *J. Climate Appl. Meteor.*, **26,** 1483–1495.

Mahrer, Y., and R. A. Pielke, 1977: The effects of topography on the sea and land breezes in a two-dimensional numerical model. *Mon. Wea. Rev.*, **105,** 1151–1162.

McCumber, M. C., 1980: A numerical simulation of the influence of heat and moisture fluxes upon mesoscale circulations. Ph.D. dissertation. University of Virginia, 255 pp.

Mellor, G. L., and T. Yamada, 1982: Development of a turbulence closure model for geophysical fluid problems. *Rev. Geophys. Space Phys.*, **20,** 851–875.

Mihailović, D. T., R. A. Pielke, B. Rajković, T. J. Lee, and M. Jeftić, 1993: A resistance representation of schemes for evaporation from bare and partly plant-covered surface for use in atmospheric models. *J. Appl. Meteor.* **32,** 1038–1054.

Miller, M. J., and Thorpe, A. J., 1981: Radiation conditions for the lateral boundaries of limited area numerical models. *Quart. J. Roy. Meteor. Soc.*, **107,** 615–628.

Modica, G. D., S. Y.-K. Yee, and J. Venuti, 1992: Some effects of soil and vegetation databases on spectra of limited-area mesoscale simulations. *Mon. Wea. Rev.*, **120,** 2067–2082.

Noilhan, J., and S. Planton, 1989: A simple parameterization of land surface processes for meteorological models. *Mon. Wea. Rev.*, **117,** 536–549.

Orlanski, I., 1976: A simple boundary condition for unbounded hyperbolic flows. *J. Comput. Phys.*, **21,** 251–269.

Paegle, J., W. G. Zdunkowski, and R. M. Welch, 1976: Implicit differencing of predictive equations of the boundary layer. *Mon. Wea. Rev.*, **104,** 1321–1324.

Paltrige, G. W., and C. M. R. Platt, 1976: *Radiative Process in Meteorology and Climatology.* Elsevier, 318 pp.

Pielke, R. A., 1984: *Mesoscale Meteorological Modeling.* Academic Press, 612 pp.

——, G. A. Dalu, J. S. Snook, T. J. Lee, and T. G. F. Kittel, 1991: Nonlinear influence of mesoscale land use on weather and climate. *J. Climate,* **4,** 1053–1069.

Pinty, J.-P., P. Mascart, E. Richard, and R. Rosset, 1989: An investigation of mesoscale flows induced by vegetation inhomogeneities using an evapotranspiration model calibrated against HAPEX–MOBILHY data. *J. Appl. Meteor.,* **28,** 976–992.

Rabin, R. M., S. Stadler, P. J. Wetzel, D. J. Stensrud, and M. Gregory, 1990: Observed effects of landscape variability on convective clouds. *Bull. Amer. Meteor. Soc.,* **71,** 272–280.

Rogers, R. R., and M. K. Yau, 1989: A short course in cloud physics. *International Series in Natural Philosophy,* Pergamon, 254 pp.

Rutledge, S. A., and P. V. Hobbs, 1984: The mesoscale and microscale structure and organization of clouds and precipitation in midlatitude cyclones. XII: A diagnostic modeling study of precipitation development in narrow cloud-frontal rainbands. *J. Atmos. Sci.,* **41,** 2949–2972.

Segal, M., R: Avissar, and M. C. McCumber, 1988: Evaluation of vegetation effects on the generation and modification of mesoscale circulations. *J. Atmos. Sci.,* **45,** 2268–2292.

Tjernström, M., 1989: Some tests with a surface energy balance scheme, including a bulk parameterisation for vegetation, in a mesoscale model. *Bound.-Layer Meteor.,* **48,** 33–68.

Yan, H., and R. A. Anthes, 1988: The effect of variations in surface moisture on mesoscale circulations. *Mon. Wea. Rev.,* **116,** 192–208.